

# Wavelength-controlled hologram-waveguide modules for continuous beam-scanning in a phased-array antenna system

Zhong Shi, Yongqiang Jiang, Brie Howley, Yihong Chen, Ray T. Chen

Microelectronics Research Center, Department of Electrical and Computer Engineering,  
The University of Texas at Austin, 10100 Burnet Road, PRC/MER/1.606G, Austin, TX 78758 USA

## Abstract

Wavelength-controlled true-time delay modules based on the dispersive hologram-waveguide are presented here to provide continuous beam-scanning for a X-band phased-array antenna system. The true-time delay modules operating in the 1550nm region were fabricated with continuously tunable time delays from 5ps to 64ps. All-optical wavelength conversion in the semiconductor optical amplifiers was proposed in the system to extend the beam-scanning scope from one dimension to two dimensions. The wavelength-controlled time delays were measured across the X-band (8-12GHz) in the experiment.

**Keywords:** Dispersion, wavelength conversion, semiconductor optical amplifier, true-time delay, phased-array antenna

## 1. Introduction

The phased-array antenna offers various advantages such as accurate and quick beam-scanning without physical movement. It has numerous applications in both military and civilian radar systems and in wireless communication systems. Optical true-time delay techniques have been extensively researched in the past few years because of their promising potential applications in phased-array antenna systems. The main advantage of using the optical true-time delay technique in phased-array antenna systems is freedom from the frequency squint effect. This effect can cause change in the beam-scanning angle, an undesirable feature for the phased-array systems. The application of the optical true-time delay technique in phased-array antenna systems offers better performance compared with the traditional electrical true-time delay technique. Optical true-time delay technique has much larger bandwidth and is freedom from the electromagnetic interference, which is often a serious problem that needs to be considered in the design of an electrical scheme. Many different optical true-time delay schemes have been proposed and demonstrated in the past few years [1,2,3]. The acoustic-optic-based optical true-time delay scheme is compact and easy to integrate. However, its bandwidth is quite limited. Chirped Bragg grating written into the fiber was used to achieve true-time delay for the antenna system. The problem associated with chirped Bragg grating is that the time delay ripple is difficult to overcome. The tradeoff between the bandwidth and the length of the grating is also a problem. Chromatic dispersion in single-mode fiber was used to produce the desired time delay for the antenna systems. But the approach requires fiber length up to several kilometers to get several picoseconds of time delay.

The hologram-waveguide-based true-time-delay technique was researched because of its advantages of low cost, high packaging density, and simple fabrication process. The digitalized true-time-delay modules using hologram-waveguide-based technique were demonstrated [4, 5], in which time delay modules were designed for working in both the 850 nm and the 1550 nm wavelength regions. A quasi-analog true-time-delay scheme was proposed and demonstrated [6], an improvement compared with digitalized schemes, but continuous time delays are available only in a narrow range.

It is desirable for true-time-delay modules to provide continuously tunable time delays with operating wavelengths in the 1550 nm region, considering their potential real applications. In this paper we present a wavelength-controlled scheme in hologram-waveguide true-time-delay modules to provide continuous beam scanning for a X-band phased-array antenna system. Time delays can be continuously tuned by varying the wavelengths in the various modules. The true-time-delay modules reported herein can provide continuous time delays from 5ps to 64ps. All-optical wavelength conversion in the

semiconductor optical amplifier was proposed to extend the beam-scanning scope from one dimension to two dimensions [7]. The wavelength-controlled time delays were measured across the X-band in the experiment.

## 2. The principle and the structure

The general configuration of the proposed scheme for wavelength-controlled time delay modules is shown in Fig. 1. The system has  $N$  discrete waveguide stripes with thicknesses of  $h_1, h_2, \dots$  and  $h_N$ , respectively. They are controlled independently by  $N$  discrete wavelengths  $\lambda_1, \lambda_2, \dots, \lambda_N$ . All waveguide stripes have the same hologram grating structure on the top surface in order to provide surface-normal fanouts. Therefore, all diffracted beams have the same diffraction angle  $\theta$  when the incident beams have the same wavelength. The  $(m+1)^{th}$  fanouts ( $m$ : bouncing number in the substrate) between the  $j^{th}$  module and the  $(j+1)^{th}$  module have a time delay  $\Delta T_{m+1}$  at the incident center wavelength  $\lambda$ . If the incident wavelength for the  $j^{th}$  module is tuned from the center wavelength  $\lambda$  to  $\lambda + \Delta\lambda$ , the diffraction angle becomes  $\theta + \Delta\theta$ , and  $\Delta\theta$  is determined by the dispersion equation, which in turn is derived from the Bragg condition [8]:

$$\Delta\theta = 2 \frac{\Delta\lambda}{\lambda} \tan(\theta/2) \quad (1)$$

This situation introduces a time delay  $\Delta\tau$  between  $\lambda$  and  $\lambda + \Delta\lambda$  for the  $(m+1)^{th}$  fanout in the module  $j$ . The following equation determines  $\Delta\tau_{m+1}$ :

$$\Delta\tau_{m+1} = \frac{2mnh_j}{c} \left[ \frac{1}{\cos(\theta + \Delta\theta)} - \frac{1}{\cos(\theta)} \right]. \quad (2)$$

Here  $n$  is the refractive index of the glass substrate. When the wavelength is tuned from  $\lambda$  to  $\lambda + \Delta\lambda'$  in the  $(j+1)^{th}$  module, the diffracted beam  $\lambda + \Delta\lambda'$  has a diffraction angle of  $\theta + \Delta\theta'$ , and  $\Delta\theta'$  is also determined by Equation (1). The time delay  $\Delta\tau'_{m+1}$  between  $\lambda$  and  $\lambda + \Delta\lambda'$  for the  $(m+1)^{th}$  fanout in the  $(j+1)^{th}$  module is determined by the same equation as (2), except that the substrate thickness  $h_j$  is replaced by  $h_{j+1}$ . The total time delay  $\Delta T'_{m+1}$  for the  $(m+1)^{th}$  fanout between adjacent modules can be continuously tuned according to the following equation depending on the wavelength tuning direction in the different modules:

$$\Delta T_{m+1} - (\Delta\tau_{m+1} + \Delta\tau'_{m+1}) \leq \Delta T'_{m+1} \leq \Delta T_{m+1} + (\Delta\tau_{m+1} + \Delta\tau'_{m+1}). \quad (3)$$

For the time delays to be continuously tuned, the maximum time delay from the  $m^{th}$  fanout has to be equal to or larger than the minimum time delay from the  $(m+1)^{th}$  fanout. In that case, the following equation should be satisfied:

$$\Delta T_m + (\Delta\tau_m + \Delta\tau'_m) \geq \Delta T_{m+1} - (\Delta\tau_{m+1} + \Delta\tau'_{m+1}). \quad (4)$$

With different delay combinations, the proposed scheme is capable of generating continuous time delays for RF beam scanning. Table 1 shows the designed time delay results for the different fanouts at the different tuning wavelengths for the two strips having eight fanouts each, with a thickness of 4.041mm and 4.482mm, respectively.

The structure of a wavelength-controlled two-dimensional phased-array antenna system is shown in Fig. 2. Wavelengths  $\lambda_1$  and  $\lambda_2$  from the tunable lasers are intensity modulated and then sent to the two hologram-waveguide true-time-delay modules, respectively. The wavelengths,  $\lambda_1$  and  $\lambda_2$ , together with CW wavelengths  $\lambda'_1$  and  $\lambda'_2$  are injected into the semiconductor optical amplifiers, in which wavelength conversion occurs. The time delay information in  $\lambda_1$  and  $\lambda_2$  is transferred to  $\lambda'_1$  and  $\lambda'_2$  via wavelength conversion whose principle will be explained in the next section. The wavelengths,  $\lambda'_1$  and  $\lambda'_2$ , are injected into the time delay modules, which is shown in Fig. 2. The outputs from the time delay modules in the second stage are detected by photo detectors and then electrically amplified. The amplified electrical signals are either analyzed by the network analyzer to determine the time delay information or connected to an antenna system to find the radiation patterns. By tuning the lasers in the first stage or in the second stage, the beam-scanning direction in the elevation direction or in the azimuth direction can be controlled separately.

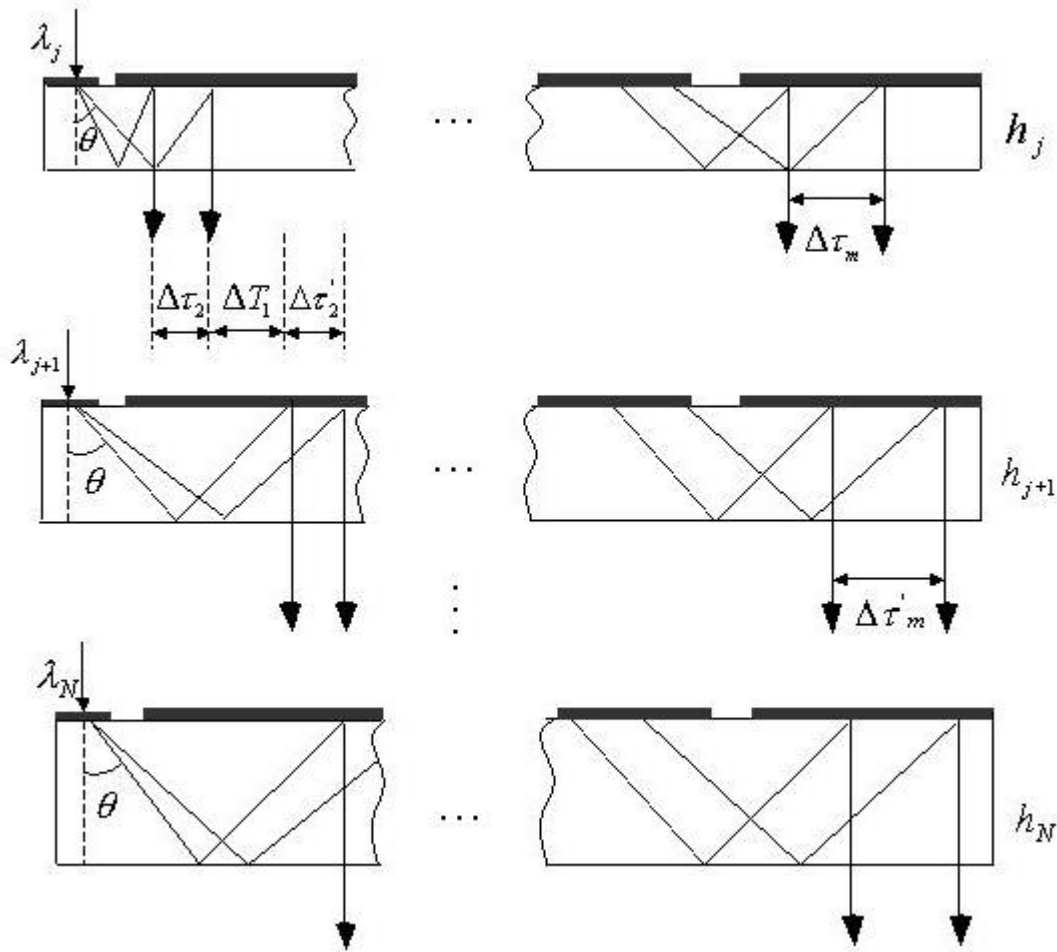


Figure 1: Configuration of the wavelength-controlled hologram-waveguide true-time delay modules

Fan out No.	Minimum time delays (ps) at	Minimum time delays (ps) at	Time delays (ps) at 1550nm	Maximum time delays (ps) at	Maximum time delays (ps) at
	$\Delta\lambda_1 = 50nm$ $\Delta\lambda_2 = -50nm$	$\Delta\lambda_1 = 30nm$ $\Delta\lambda_2 = -30nm$	$\Delta\lambda_1 = 0nm$ $\Delta\lambda_2 = 0nm$	$\Delta\lambda_1 = -30nm$ $\Delta\lambda_2 = 30nm$	$\Delta\lambda_1 = -50nm$ $\Delta\lambda_2 = 50nm$
1	2.205	2.205	2.205	2.205	2.205
2	5.435	6.575	8.235	9.895	11.035
3	8.665	10.945	14.265	17.585	19.865
4	11.895	15.314	20.295	25.276	28.695
5	15.125	19.744	26.325	32.966	37.525
6	18.355	24.053	32.355	40.657	46.355
7	21.584	28.420	38.384	48.348	55.184
8	24.810	32.789	44.414	56.039	64.018

Table 1: Designed true-time delay results at different incident wavelengths

All-optical wavelength conversion refers to transferring data information from one wavelength to another wavelength without optical-electrical-optical (O-E-O) conversion. Since wavelength conversion is in the optical domain, the potential complexity of O-E-O conversion within the communication systems could be greatly reduced. There are several different schemes for realizing wavelength conversion, such as cross-gain modulation (XGM) in semiconductor optical amplifier, cross-phase modulation (XPM) in semiconductor optical amplifier, and four-wave mixing (FWM) in semiconductor optical amplifier [9], [10], [11]. The wavelength conversion based on cross-gain modulation in semiconductor optical amplifier (SOA) was used in our experiment because of its ease of operation. Cross-gain modulation uses the nonlinear gain saturation effect in semiconductor optical amplifier to transfer data information from modulated light to CW light. The working principle may be briefly summarized as follows: the incoming intensity-modulated light  $\lambda_1$  modulates the gain of the semiconductor optical amplifier via the gain saturation effect. The CW light at the desired output wavelength  $\lambda_2$  is modulated by gain variation, which is in turn caused by the modulated light  $\lambda_1$ . So the data information is transferred from modulated light  $\lambda_1$  to CW light  $\lambda_2$  via gain variation in the semiconductor optical amplifier. The detailed analysis of the working mechanism of cross-gain modulation in semiconductor optical amplifier can be found in [9]. The converted signal in  $\lambda_2$  is phase-inverted compared with the original signal in  $\lambda_1$ . But phase-inversion does not affect the true-time delays between the modules since all the signals have phase-inversion.

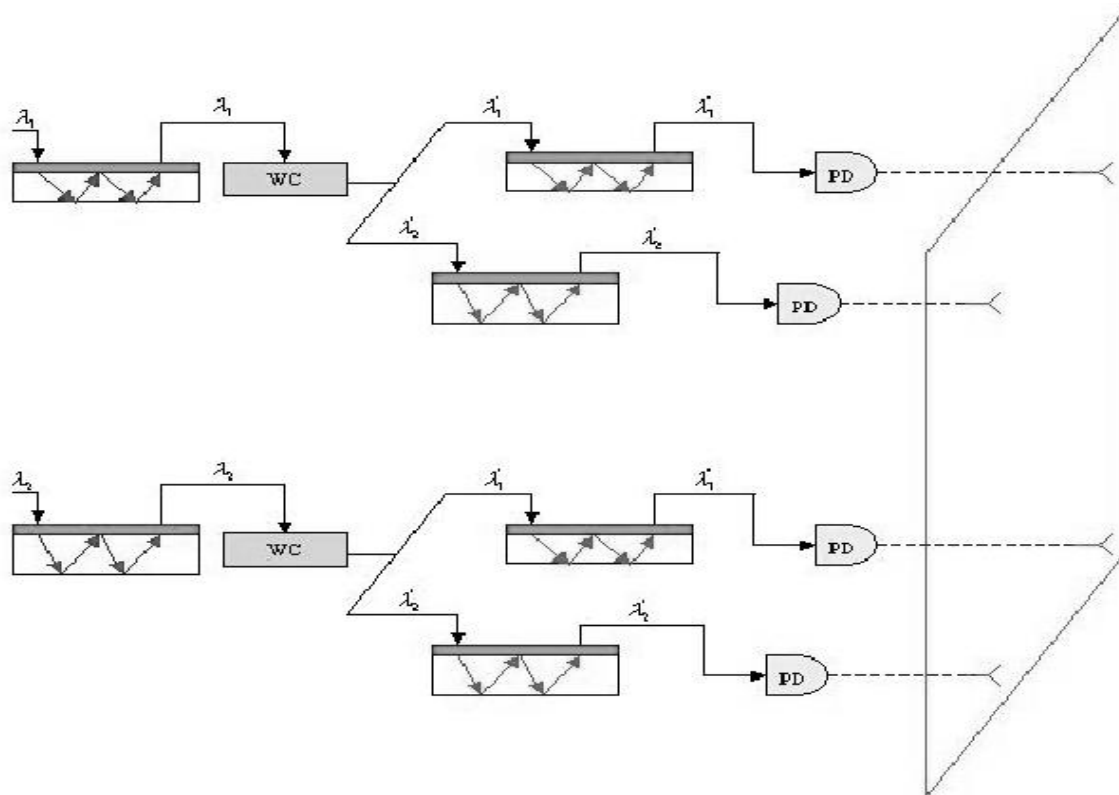


Fig. 2. Structure of a wavelength-controlled two-dimensional phased-array antenna system

### 3. Experimental results

A wide-wavelength tuning range is important to get the desired time delays since wavelength-tuning is used in the true-time delay modules. The gain bandwidth of the semiconductor optical amplifier has to be wide enough to make possible a sufficient wavelength tuning range. The measured gain vs. wavelength is shown in Fig. 3. The 3-dB gain bandwidth of semiconductor optical amplifiers is about 60nm, quite desirable for wavelength conversion within such a wide gain bandwidth. The measured frequency response and the measurement setup of cross-gain modulation in semiconductor optical amplifier are shown in Fig. 4. The measurement was made using cross-gain modulation with a counter-propagation scheme in which optical filters were eliminated in the setup. The electrical signals from the photo detectors were analyzed by a microwave spectrum analyzer (MSA).

To verify the designed result of time delay, we used the experimental setup shown in Fig. 5 to measure the RF phase vs RF frequency curves. An HP network analyzer (8510C) was used to provide an X-band RF signal and to measure the time delays in the experiment. A Santec tunable laser was modulated by a  $LiNbO_3$  external modulator and the modulated signal was fed into one of the true-time delay modules  $h_1$  (4.041mm) or  $h_2$  (4.482mm). After desired time delays within the module, the output was fed into the high-speed p-i-n photodetector connected with post-amplifier (PAs). The phase of the electrical signal from the post amplifier was measured by the HP network analyzer. We measured the 7<sup>th</sup> (m=6) fan-out for both modules in the experiment. The results of RF phase vs RF frequency are shown in Fig. 6. The time delays obtained from the above measurement are 28ps at  $\lambda_1=1580\text{nm}$  for  $h_1$  and  $\lambda_2=1520\text{nm}$  for  $h_2$ , 38ps at  $\lambda_1=1550\text{nm}$  for  $h_1$  and  $\lambda_2=1550\text{nm}$  for  $h_2$ , 48ps at  $\lambda_1=1520\text{nm}$  for  $h_1$  and  $\lambda_2=1580\text{nm}$  for  $h_2$ .

### 4. Conclusion

Wavelength-controlled hologram-waveguide true-time delay modules were presented herein. The application to a two-dimensional X-band phased-array antenna system is proposed in the paper. The wavelength-controlled time delays were measured across the X-band in the experiment.

### Acknowledgement

The support from AFOSR and MDA is acknowledged. Special thanks to Ms. Wanda Miller for her polishing the text of the whole paper.

### References

1. L. H. Gesell, R. E. Feinleib, J. L. Lafuse, T. M. Turpin, "Acoustooptic control of time delays for array beam steering," Proc., SPIE, Optoelectronic Signal Processing for Phase-Array Antenna IV, Vol. 2155, 1994, pp. 194-204.
2. A. Molony, C. Edge, I. Bennion, "Fiber grating time delay element for phased array antennas," Electronics Letters, 31, 1485, 1995.
3. A. M. Levine, "Use of fiber optical frequency and phase determining element in radar," Proc. of the 33<sup>rd</sup> Annual Symposium on Frequency Control, IEEE, 436, 1979.
4. R. Li, Z. Fu, R. Chen, "High Packing Density 2.5-THz True-Time-Delay Lines Using Spatially Multiplexed Substrate Guided Waves in Conjunction with Volume Holograms on a Single Substrate," J. L. T., Vol. 15, pp. 2253-2258, 1997.
5. Y. Chen, R. T. Chen, "A fully packaged true time delay modules for phase array antenna demonstration," IEEE Photonics Technology Letters, Vol. 14, pp. 1175-1177, Aug. 2002.
6. Z. Fu, C. Zhou, R. T. Chen, "Waveguide-hologram-based wavelength-multiplexed pseudoanalog true-time-delay module for wideband phased-array antennas," Applied Optics, Vol. 38, No. 14, pp. 3053-3059, May 1999.
7. S. Yegnanarayanan, B. Jalali, "Wavelength-selective true time delay for optical control of phased-array antenna," IEEE Photonics Technology Letter, Vol. 12, No. 8, 1049-1051, August 2001.
8. H. Kogelnik, "Coupled wave theory for thick hologram gratings," The Bell System Technical Journal, Vol. 48, pp. 2909-2947, Nov. 1969.
9. T. Durhuus, B. Mikelsen, C. Joergensen, S. L. Danielsen, K. E. Stubkjaer, "All-optical wavelength conversion by semiconductor optical amplifiers," Vol. 14, No. 6, 942-954, June 1996.
10. T. Durhuus, C. Joergensen, B. Mikelsen, R. J. S. Pedersen, and K. E. Stubkjaer, "All optical wavelength conversion by SOA's in a Mach-Zehnder configuration," IEEE Photonics Technol. Lett., Vol. 6, pp. 53-55, Jan. 1994.
11. G. Grosskopf, R. Ludwig, R. Schnabel, and H. G. Weber, "Frequency conversion with semiconductor laser amplifiers for coherent optical frequency division switching," Proc. IOOC'89, Kobe, Japan, July 1989, Paper 19C4-4

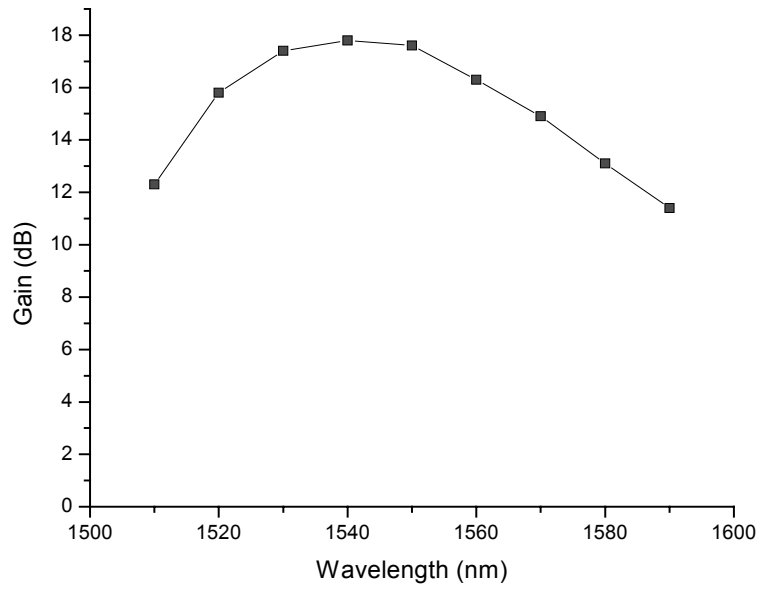


Fig. 3. The measured results of gain vs. wavelength

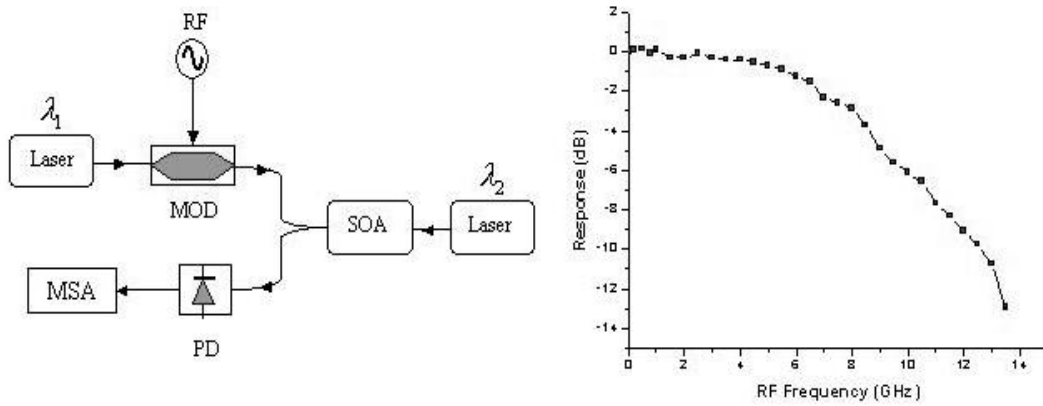


Fig. 4. The measured results of the frequency response

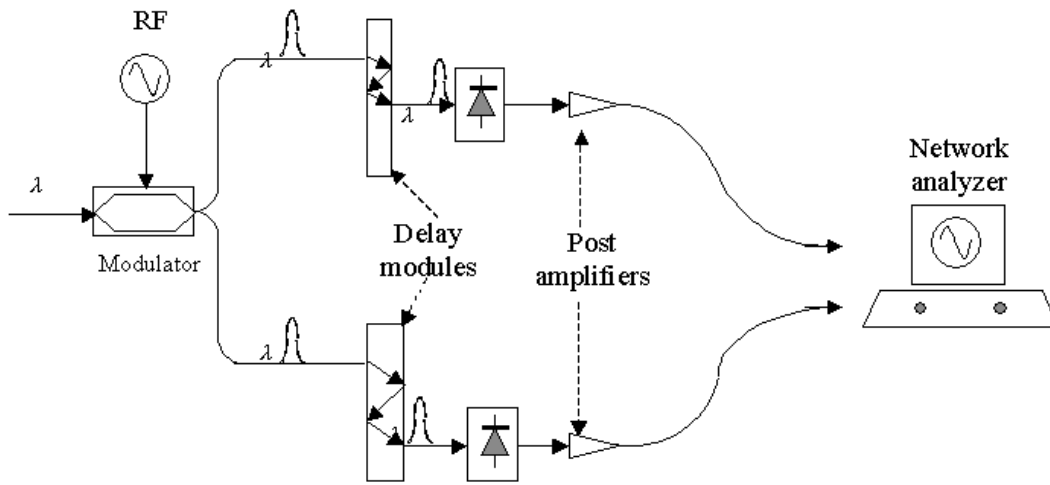


Fig. 5. The setup for measuring time delays

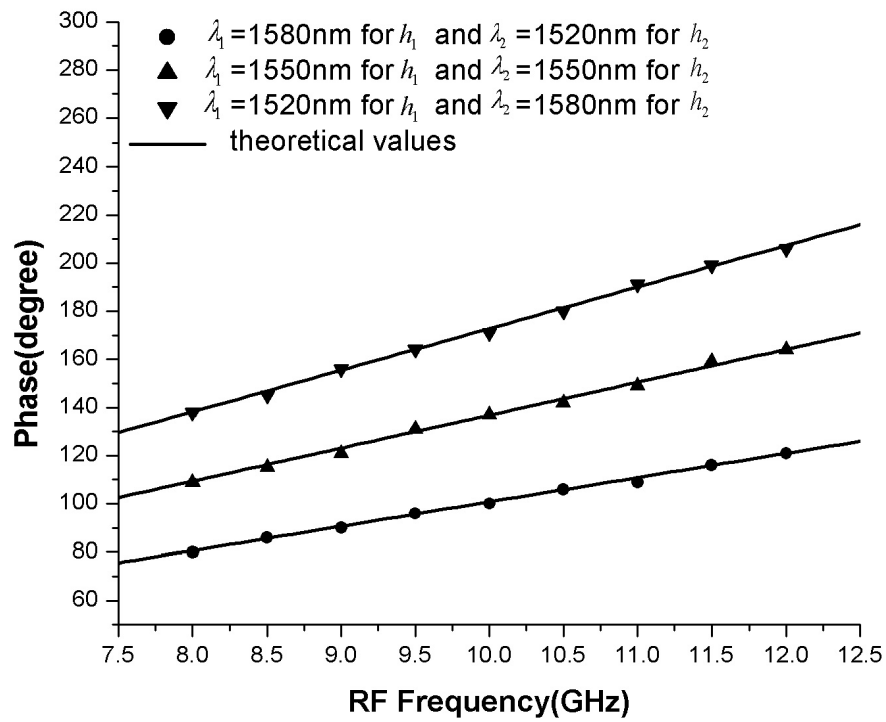


Fig. 6. The measured RF phase vs. RF frequencies